

# Quantum computing with error mitigation for data-driven computational mechanics

Zengtao Kuang<sup>a,†</sup>, Yongchun Xu<sup>a,†</sup>, Qun Huang<sup>a</sup>, Jie Yang<sup>a</sup>,  
Chafik El Kihal<sup>a</sup>, Heng Hu<sup>a,\*</sup>

<sup>a</sup>School of Civil Engineering, Wuhan University, 8 South Road of East Lake, Wuchang, 430072  
Wuhan, PR China

## Abstract

As a crossover frontier of physics and mechanics, quantum computing is showing its great potential in computational mechanics. However, quantum hardware noise remains a critical barrier to achieving accurate simulation results due to the limitation of the current hardware level. In this paper, we integrate error-mitigated quantum computing in data-driven computational mechanics, where the zero-noise extrapolation (ZNE) technique is employed to improve the accuracy of quantum computing. Numerical examples including multiscale simulation of a composite L-shaped beam are conducted with the quantum computer simulator Qpanda, and the results validate the effectiveness of the proposed method. We believe this work presents a promising step towards using the power of quantum computing in computational mechanics.

**Keywords:** Quantum computing; Data-driven computational mechanics; Error mitigation; Zero-noise extrapolation; Distance calculation.

## 1 Introduction

Due to the unique properties of quantum systems like superposition and entanglement, quantum computing enables exponentially reducing the complexity of computation in certain tasks. It has attracted the increasing attention of researchers in the field of computational mechanics. Until now, quantum computing has been applied to solve, e.g., boundary value problems with finite element method [1], Poisson's equations [2], fluid dynamics [3], composite materials [4] and so on. Recently, Xu et al. [5] introduced a quantum computing enhanced data-driven computational mechanics, which was validated both in a quantum computer simulator and a real quantum computer. However, the noise remains one of the limitations of the current quantum hardware, which prevents taking advantage of quantum computing. In this work, we focus on the noise issue of hardware, aiming to improve the accuracy of quantum computing for data-driven computational mechanics.

Data-driven computational mechanics (DDCM) is a novel approach to solving boundary value problems (BVP) in the domain of mechanics [6]. In this computing paradigm, the simulation is conducted by using material data directly, therefore bypassing the need for material

---

<sup>†</sup>These authors contributed equally to this work.

\*Corresponding author. E-mail address: huheng@whu.edu.cn.

modeling. It has been rapidly extended in the fields of multiscale simulation [7–12], dynamics [13], structural stability [14, 15], fracture [16, 17], hyperelasticity [18, 19], local refinement problems [20–22], and so on. DDCM relies on iteratively shortening the distance between material data and conservation laws, which requires nearest-neighbor searches in a material database concerning numerous distance calculations. Specifically, if a nearest-neighbor search is performed in a material database with  $N$  data, each having dimension  $D$ , then  $N$  distance calculations are required, each with a cost  $O(D)$ , leading to a computational complexity of  $O(ND)$ . In DDCM involving a high-dimension and high-density material database, the distance calculations become a computational bottleneck [23].

The emergence of the quantum computer shows promise in accelerating distance calculation in DDCM. In the work of Xu et al. [5], a quantum computing enhanced data-driven computational mechanics (referred to as qDD) is introduced, which exponentially reduces the complexity of distance calculation from  $O(D)$  to  $O(\log D)$ . However, qDD assumes the usage of a fault-tolerant quantum computer [24], and quantum hardware noise is not considered. The hardware noise in quantum computers usually originates from unexpected interactions with the environment and imperfect gate operations [25]. For instance, environmental disturbances can lead to decoherence in a quantum system, resulting in the loss of information. Different from classical computers, quantum computers are prone to output inaccurate information even with small disturbance [26]. The reason is that the quantum bits (qubits) in quantum computers, unlike classical bits confined to 0 and 1, can be any superposition of  $|0\rangle$  and  $|1\rangle$ . Therefore, addressing the error caused by the hardware noise is a crucial issue for the application of quantum computing.

The primary objective of this paper is to address the quantum hardware noise issue in the qDD. Currently, there are two kinds of quantum algorithms that can be considered to achieve the goal [26]. The first is quantum error correction (QEC), which offers a solution by redundantly encoding quantum information with additional qubits and actively detecting and correcting errors [25, 27], resulting in fault-tolerant computing. Unfortunately, the hardware level of quantum computers is now in the era named Noisy Intermediate-Scale Quantum (NISQ) [28], meaning the number of qubits is limited. However, QEC requires a large overhead number of additional qubits, making it infeasible for NISQ quantum computers [26, 28]. The second approach, quantum error mitigation (QEM), emerges as a more practical alternative for NISQ devices [29]. One prominent QEM method is zero-noise extrapolation (ZNE), which intentionally introduces additional noise and extrapolates results to the zero-noise limit [30, 31]. An advantage of ZNE is its independence from additional qubits, rendering it well-suited for NISQ quantum computers. It has been proved to improve the accuracy of a noisy superconducting quantum processor to an inaccessible level [32]. Notably, IBM Quantum recently demonstrated the utility of NISQ quantum computers before the fault-tolerant era with the help of ZNE, which passes a calculation milestone in the field of quantum computing [33, 34].

In this paper, ZNE is applied to mitigate the quantum hardware noise within qDD, aiming to improve the accuracy of distance calculation, thereby enhancing the overall performance of qDD when operating on a noisy quantum computer. Furthermore, the  $k$ -d tree data structure

[23, 35–37] is used to reduce the number of distance calculations, resulting in a more favorable computational complexity. The quantum computer simulator Qpanda [38] is utilized to validate the proposed approach, which allows one to execute quantum algorithms on classical computers. Several numerical experiments are conducted to confirm the effectiveness of ZNE in improving the accuracy of distance calculation. Moreover, we present a data-driven multiscale simulation of a composite L-shaped beam to illustrate the practical utility of the proposed methodology.

The remainder of this article is laid out as follows. In Section 2, we revisit the fundamental formulations of data-driven computational mechanics and the quantum algorithm for distance calculation. Subsequently, the application of ZNE in reducing quantum hardware noise is demonstrated. In Section 3, we present numerical examples to validate the effectiveness of ZNE in improving the accuracy of distance calculation. Additionally, we use a roof truss as a case study to emphasize the impact of ZNE on the performance of data-driven computing on a noisy quantum computer. A multiscale simulation of a composite L-shaped beam is presented in Section 4 as an application example, and some conclusions and discussions are provided in Section 5.

## 2 Methodology

In Section 2.1, we briefly introduce the formulations of data-driven computational mechanics. This computing scheme involves computationally expensive distance calculations for nearest-neighbor searches. Therefore, the quantum algorithm for distance calculation is then introduced in Section 2.2 to reduce the computational complexity. Finally, the formulations of ZNE for mitigating the influence of hardware noise are introduced in Section 2.3.

### 2.1 Data-driven computing

We consider a structure of elastic solid, and its configuration is discretized with finite elements. At each integration point  $e$ , the data-driven solver seeks to minimize the distance between the corresponding stress-strain data  $\bar{\mathbf{z}}_e^* = (\bar{\boldsymbol{\epsilon}}_e^*, \bar{\boldsymbol{\sigma}}_e^*)$  in the material database  $\bar{\mathcal{D}}$  and the admissible stress-strain state  $\bar{\mathbf{z}}_e = (\bar{\boldsymbol{\epsilon}}_e, \bar{\boldsymbol{\sigma}}_e)$  that satisfies equilibrium and compatibility. A distance-based functional formulates this constrained minimization problem

$$\Pi = \frac{1}{2} \sum_{e=1}^m w_e \bar{\mathcal{F}}_e(\bar{\mathbf{z}}_e, \bar{\mathbf{z}}_e^*) - \bar{\boldsymbol{\eta}}^T \left( \sum_{e=1}^m w_e \bar{\mathbf{B}}_e \bar{\boldsymbol{\sigma}}_e - \bar{\mathbf{f}} \right) \quad (1)$$

where the distance is defined as

$$\bar{\mathcal{F}}_e(\bar{\mathbf{z}}_e, \bar{\mathbf{z}}_e^*) = (\bar{\boldsymbol{\epsilon}}_e - \bar{\boldsymbol{\epsilon}}_e^*)^T \bar{\mathbb{C}} (\bar{\boldsymbol{\epsilon}}_e - \bar{\boldsymbol{\epsilon}}_e^*) + (\bar{\boldsymbol{\sigma}}_e - \bar{\boldsymbol{\sigma}}_e^*)^T \bar{\mathbb{C}}^{-1} (\bar{\boldsymbol{\sigma}}_e - \bar{\boldsymbol{\sigma}}_e^*) \quad (2)$$

Here,  $\bar{\boldsymbol{\eta}}$  is a vector of Lagrange multipliers enforcing the equilibrium constraints,  $\bar{\mathbf{B}}_e$  is a matrix of interpolation functions,  $\bar{\mathbf{f}}$  denotes the vector of the nodal force,  $w_e$  denotes the integration weight and  $m$  is the total number of integration points. Note that  $\bar{\mathbb{C}}$  is a user-defined symmetric

matrix to scale stress and strain to a similar magnitude, and it does not represent a material behavior.

We take all possible variations of Eq. (1) considering the compatibility constraints  $\bar{\epsilon}_e = \bar{\mathbf{B}}_e \bar{\mathbf{u}}$ , resulting in the following linear equations

$$\sum_{e=1}^m w_e \bar{\mathbf{B}}_e^T \bar{\mathbf{C}} \bar{\mathbf{B}}_e \bar{\mathbf{u}} = \sum_{e=1}^m w_e \bar{\mathbf{B}}_e^T \bar{\mathbf{C}} \bar{\epsilon}_e^* \quad (3a)$$

$$\sum_{e=1}^m w_e \bar{\mathbf{B}}_e^T \bar{\mathbf{C}} \bar{\mathbf{B}}_e \bar{\boldsymbol{\eta}} = \bar{\mathbf{f}} - \sum_{e=1}^m w_e \bar{\mathbf{B}}_e^T \bar{\boldsymbol{\sigma}}_e^* \quad (3b)$$

The data-driven computing starts by randomly selecting data  $\bar{\mathbf{z}}_e^*$  from the database  $\bar{\mathcal{D}}$  for each integration point, followed by iterative computing containing two steps. The first step is a mapping operation from  $\bar{\mathbf{z}}_e^*$  to  $\bar{\mathbf{z}}_e$  by solving the linear problem in Eq. (3). The second step is a reverse mapping from  $\bar{\mathbf{z}}_e$  to  $\bar{\mathbf{z}}_e^*$  via nearest-neighbor search, and the aim is to find the closest material data  $\bar{\mathbf{z}}_e^*$  in the database for each admissible data  $\bar{\mathbf{z}}_e$

$$\bar{\mathcal{F}}_e(\bar{\mathbf{z}}_e, \bar{\mathbf{z}}_e^*) \leq \bar{\mathcal{F}}_e(\bar{\mathbf{z}}_e, \bar{\mathbf{z}}_e'), \quad \forall \bar{\mathbf{z}}_e' \in \bar{\mathcal{D}} \quad (4)$$

It requires distance calculations between  $\bar{\mathbf{z}}_e$  and all the data  $\bar{\mathbf{z}}_e' \in \bar{\mathcal{D}}$ , then the optimal data  $\bar{\mathbf{z}}_e^*$  is set to be the data  $\bar{\mathbf{z}}_e'$  corresponding to the minimum distance. The iteration stops when the distance between  $\bar{\mathbf{z}}_e$  to  $\bar{\mathbf{z}}_e^*$  is minimized for each integration point, resulting in the final solution of the simulation.

It should be emphasized that the nearest-neighbor search consumes a tremendous computational cost of distance calculation for a high-dimensional and high-density database. For the nearest-neighbor search involving a database containing  $N$  data, and the dimension of the data is  $D$ , the complexity of the brute-force search on a classical computer requires  $N$  times distance calculations, each with a complexity of  $O(D)$ , resulting in a total complexity of  $O(ND)$ . Related works show that efficient data structures can reduce the complexity [23, 35–37, 39] without significant loss of accuracy in data-driven computing. For instance, the  $k$ -d tree can reduce the number of distance calculations, resulting in a complexity of approximately  $O(\log(N)D)$  [35]. To further reduce the computational cost, the  $k$ -d tree will be used in this work, incorporating the quantum algorithm for distance calculation introduced in the next section.

## 2.2 Distance calculation via quantum computing

In this section, we recall the quantum algorithm for distance calculation. For simplicity, we denote the scaled admissible data  $\bar{\mathbf{z}}_e$  as a vector  $\mathbf{V}$  and the scaled material data  $\bar{\mathbf{z}}_e'$  a vector  $\mathbf{V}'$ , and their dimensions are both  $D$ . Then, we can rewrite the distance in Eq. (2) as a squared Euclidean distance  $d$

$$d = |\mathbf{V} - \mathbf{V}'|^2 \quad (5)$$

The quantum algorithm for computing  $d$  is introduced in the following.

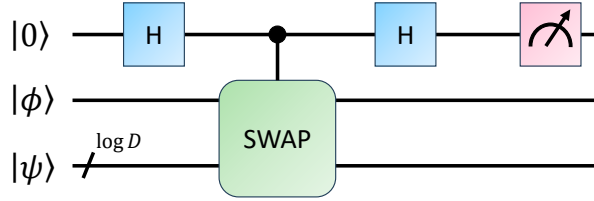


Figure 1: Quantum circuit of the swap test.

First, two quantum states containing the information of  $\mathbf{V}$  and  $\mathbf{V}'$  are encoded into the quantum computer via qRAM [40, 41]

$$|\phi\rangle = \frac{1}{\sqrt{Z}}(|\mathbf{V}\rangle|0\rangle - |\mathbf{V}'\rangle|1\rangle) \quad (6a)$$

$$|\psi\rangle = \frac{1}{\sqrt{2}}(|0\rangle|\mathbf{V}\rangle + |1\rangle|\mathbf{V}'\rangle) \quad (6b)$$

where the Dirac notation  $|\cdot\rangle$  denotes a quantum state, and  $Z = |\mathbf{V}|^2 + |\mathbf{V}'|^2$ . In addition,  $|\mathbf{V}\rangle$  and  $|\mathbf{V}'\rangle$  denote the normalized  $\mathbf{V}$  and  $\mathbf{V}'$ , respectively. Second, the swap test [42] is used to compute the inner product  $|\langle\phi|\psi\rangle|^2$ , which includes two Hadamard gates and one CSWAP gate. The corresponding quantum circuit is shown in Figure 1. Note that the swap test consists of only three gates and has a computational complexity of  $O(1)$ , independent of  $D$ . At the end of the circuit, the probability of the measurement result of the first qubit being  $|0\rangle$  is

$$p = \frac{1}{2} + \frac{1}{2}|\langle\phi|\psi\rangle|^2 \quad (7)$$

Finally, the average squared distance is obtained by

$$d = 4Z(p - \frac{1}{2}) \quad (8)$$

To compute  $d$  using Eq. (8), we need to obtain  $Z$  and  $p$ , where  $Z$  is pre-computed in the classical computer [5] and  $p$  is calculated by running the swap test circuit. Due to the unique nature of the quantum system [25], measurement leads to the collapse of the quantum state, resulting in the acquisition of only one bit of classical information. Consequently, it requires repeated circuit running to read out  $p$ , and it is estimated statistically [5]. Suppose we have  $n_s$  measurements, and the number of  $|0\rangle$  in the measurement results is  $n_0$ . Then  $p$  is estimated by  $\hat{p} = n_0/n_s$ , where  $\hat{p}$  denotes an estimated value for  $p$ .

Thanks to the advantage of quantum computers in manipulating vectors and tensor products in high-dimensional spaces, the computational complexity of distance calculation is reduced from  $O(D)$  in classical computing to  $O(\log D)$  in quantum computing. With the help of the quantum algorithm, the complexity of the nearest-neighbor search in data-driven computing is reduced to  $O(D + N \log(D))$  [5]. Furthermore, the simulations in this work are conducted with the  $k$ -d tree structure presented in Appendix B to reduce the number of queries at the same time, resulting in a more favorable complexity  $O(D + \log(N) \log(D))$ .

### 2.3 Zero-noise extrapolation

While quantum computing has demonstrated a remarkable exponential reduction in computational complexity, the accuracy of current devices of quantum computing is influenced by hardware noise [32], leading to challenges in extracting precise and effective information. Specifically, the estimated  $\hat{p}$  will be biased from the true value, causing an error in the calculated distance. Since fault-tolerant quantum computers are not yet available [28], the zero-noise extrapolation method is applied to improve the accuracy of the distance calculation. It offers a way to mitigate quantum hardware noise without the need for additional qubit resources and detailed knowledge of quantum processors. The main idea of ZNE is to intentionally scale up the hardware noise so as to obtain the estimated  $\hat{p}$  with different noise levels, and then the obtained results are used to extrapolate the noiseless value. In the following, we will introduce the details of ZNE, which can be implemented in two steps: noise-scaling and extrapolation [43].

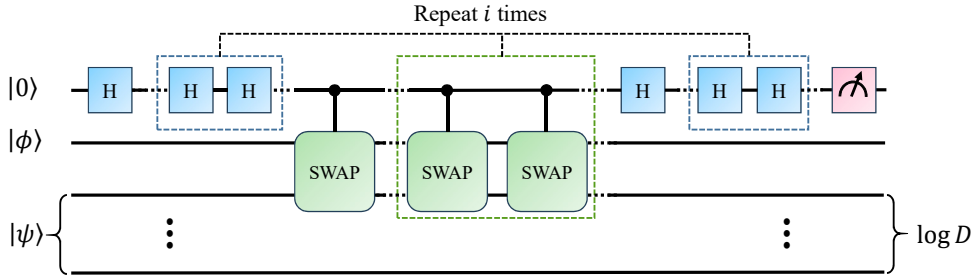


Figure 2: The sketch of the folding circuit.

The first step aims to scale up the hardware noise while still allowing the quantum circuit to perform the swap test. To achieve this, the quantum circuit requires to be modified by folding each quantum gate  $U$

$$U \longrightarrow U(U^\dagger U)^i \quad (9)$$

where  $U^\dagger$  is the conjugate of  $U$  and  $i$  is a positive integer representing the number of foldings. If all the gates are noiseless, the gate folding has no effect on the final output since  $U^\dagger U$  is equal to the identity operator [25]. However, on a quantum computer with hardware noise, the gate folding will lead to an increasing noise with a factor  $\lambda = 1 + 2i$ , which corresponds to the total number of gates in the folding circuit. Hence, we can construct a folding circuit by repeating each gate of the swap test (see Figure 2), and perform measurements on the quantum circuit to get the estimated probability  $\hat{p}$  with higher noise. By controlling the number of foldings  $i$  from 0 to a maximum folding number  $n$  to build a set of quantum circuits, we can get the estimated  $\hat{p} = \{\hat{p}_0, \hat{p}_1, \dots, \hat{p}_n\}$  corresponding to a set of noise scale factors  $\lambda = \{1, 3, \dots, 1 + 2n\}$ .

In the following, we will illustrate the influence of gate folding on the estimated  $\hat{p}$  in noisy quantum computing, which requires deriving the relation between  $\hat{p}$  and  $\lambda$ . Here, we use the density matrix for derivation, which can be used to describe the mixed quantum state concerning decoherence. The depolarizing channel [44] is employed to simulate the hardware noise, which is an important type of noise [45, 46] to describe the phenomenon of quantum systems transitioning

from pure states to mixed states. Firstly, we consider a single qubit density matrix  $\rho$ , whose evolution with an noiseless gate  $U$  is expressed as

Noiseless gate:

$$\rho \xrightarrow{U} U\rho U^\dagger \quad (10)$$

Then we consider the hardware noise of depolarizing channel. If we define that the probability of qubit being depolarized is  $q$ , then a noisy gate  $U$  applying to the density matrix can be described as

Noisy gate ( $\lambda = 1$ ):

$$\rho \xrightarrow{U} (1 - \frac{3}{4}q)U\rho U^\dagger + \frac{q}{4} \sum_{j=1}^3 (UG_j)\rho(UG_j)^\dagger, \quad G = \{X, Y, Z\} \quad (11)$$

where  $G = \{X, Y, Z\}$  are three Pauli gates, respectively to a rotation around the  $x$ ,  $y$  and  $z$  axes of the Bloch sphere by  $\pi$  radians [25]. For simplification, the second term of Eq. (11) is set as  $\rho^*(q) = \frac{q}{4} \sum_{j=1}^3 (UG_j)\rho(UG_j)^\dagger$ , which represents a mixed state. Then Eq. (11) can be rewritten as

Noisy gate ( $\lambda = 1$ ):

$$\rho \xrightarrow{U} (1 - \frac{3}{4}q)U\rho U^\dagger + \rho^*(q) \quad (12)$$

Now we consider folding the gate once, which means we need to apply two additional gates  $U^\dagger$  and  $U$ . First, we apply the noisy gate  $U^\dagger$

Noisy gate ( $\lambda = 2$ ):

$$\begin{aligned} \rho &\xrightarrow{UU^\dagger} (1 - \frac{3}{4}q)U^\dagger((1 - \frac{3}{4}q)U\rho U^\dagger + \rho^*(q))U + \\ &\quad \frac{q}{4} \sum_{j=1}^3 (UG_j)^\dagger((1 - \frac{3}{4}q)U\rho U^\dagger + \rho^*(q))(UG_j) \\ &= (1 - \frac{3}{4}q)^2\rho + (1 - \frac{3}{4}q)U^\dagger\rho^*(q)U + \\ &\quad \frac{q}{4} \sum_{j=1}^3 (UG_j)^\dagger((1 - \frac{3}{4}q)U\rho U^\dagger + \rho^*(q))(UG_j) \\ &= (1 - \frac{3}{4}q)^2\rho + \rho^*(q, q^2) \end{aligned} \quad (13)$$

where  $\rho^*(q, q^2)$  is a density matrix related to the linear combination of  $q$  and  $q^2$ . Then we

consider another noisy gate  $U$  to finish the folding

Noisy gate ( $\lambda = 3$ ):

$$\begin{aligned}
\rho &\xrightarrow{UU^\dagger U} (1 - \frac{3}{4}q)U((1 - \frac{3}{4}q)^2\rho + \rho^*(q, q^2))U^\dagger + \\
&\quad \frac{q}{4}\sum_{j=1}^3(UG_j)((1 - \frac{3}{4}q)^2\rho + \rho^*(q, q^2))(UG_j)^\dagger \\
&= (1 - \frac{3}{4}q)^3U\rho U^\dagger + (1 - \frac{3}{4}q)U\rho^*(q, q^2)U^\dagger + \\
&\quad \frac{q}{4}\sum_{j=1}^3(UG_j)((1 - \frac{3}{4}q)^2\rho + \rho^*(q, q^2))(UG_j)^\dagger \\
&= (1 - \frac{3}{4}q)^3U\rho U^\dagger + \rho^*(q, q^2, q^3)
\end{aligned} \tag{14}$$

One can see that after folding once,  $\rho^*$  is related to a higher order of  $q^3$ . Furthermore, if we consider folding  $n$  times, the derivation of the folding can be generalized as

Noisy gate ( $\lambda = 1 + 2n$ ):

$$\rho \xrightarrow{U(U^\dagger U)^n} (1 - \frac{3}{4}q)^\lambda U\rho U^\dagger + \rho^*(q, q^2, \dots, q^\lambda) \tag{15}$$

Eq. (15) corresponds to the folding of a single-qubit gate. Moreover, we generalize the gate folding for the circuit of the swap test, which concerns two Hadamard gates acting on a single qubit and one CSWAP gate acting on three qubits. Therefore, there will be 5 times of single depolarizing acting on the qubits

Noisy circuit ( $\lambda = 1 + 2n$ ):

$$\rho \xrightarrow{\text{SWAP TEST}} (1 - \frac{3}{4}q)^{5\lambda} U\rho U^\dagger + \rho^*(q^1, q^2, \dots, q^{5\lambda}) \tag{16}$$

where the density matrix  $\rho$  is considered as the outer product [25] of the initial quantum state  $|0\phi\psi\rangle\langle 0\phi\psi|$ . To obtain the probability of the first qubit measured to be  $|0\rangle$ , we need to sum the related diagonal elements of the final density matrix in Eq. (16)

$$\hat{p}(\lambda) = (1 - \frac{3}{4}q)^{5\lambda} p + \sum_{j=1}^{5\lambda} p_j^* q^j \tag{17}$$

where  $\hat{p}$  is the probability concerning hardware noise,  $p$  is the true probability computed from the density matrix  $U\rho U^\dagger$ , and  $p_j^*$  are values computed from  $\rho^*(q^1, q^2, \dots, q^{5\lambda})$ . One notes that the coefficient of the first term  $(1 - \frac{3}{4}q)^{5\lambda}$  will approach zero with the increasing noise scale factor  $\lambda$ , which means the information of  $p$  gradually loses. In addition, this theoretical derivation is different from that in the work of Giurgica-Tiron et al. [43]. The reason is that their derivation is under the assumption of global depolarizing noise affecting all qubits, while this work considers depolarizing noise for each single qubit.



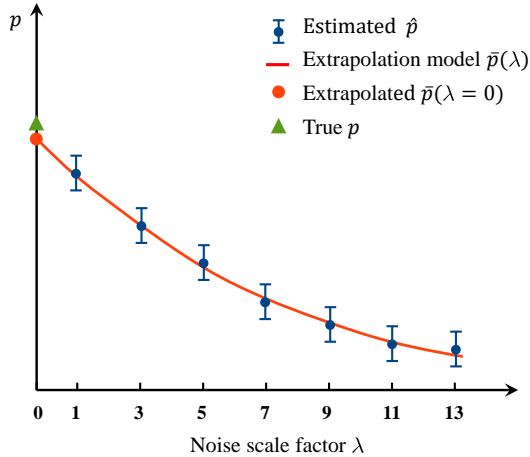


Figure 3: The sketch of the extrapolation method.

The second step of ZNE intends to extrapolate the noiseless probability based on the estimated  $\hat{\mathbf{p}} = \{\hat{p}_0, \hat{p}_1, \dots, \hat{p}_n\}$  under different noise scale factors  $\boldsymbol{\lambda} = \{1, 3, \dots, 1 + 2n\}$ . As shown in Figure 3, this extrapolation requires a model  $\bar{p}(\lambda)$  to characterize the relationship between  $\hat{p}$  and  $\lambda$ . After fitting this model with  $\hat{\mathbf{p}}$  and  $\boldsymbol{\lambda}$ , the noiseless value is predicted as  $\bar{p}(\lambda = 0)$ . One straightforward thought is to directly use a similar form in Eq. (17) as the extrapolation model, since it is the exact relationship between  $\hat{p}$  and  $\lambda$ . However, it is hard to find a similar and easy-to-fit form, because the number of terms in  $\sum_{j=1}^{5\lambda} p_j^* q^j$  changes depending on the value of  $\lambda$ . Another approach is to assume a relatively concise model between the estimated  $\hat{p}$  and the noise scale factor  $\lambda$ , which may be the core concept of ZNE. Here, we present four extrapolation models, i.e., linear extrapolation, quadratic extrapolation, exponential extrapolation and Richardson extrapolation, which are commonly used in ZNE [43]

$$\begin{aligned}
 \text{Linear extrapolation :} & \quad \bar{p}^{\text{linear}}(\lambda) = c_0 + c_1\lambda \\
 \text{Quadratic extrapolation :} & \quad \bar{p}^{\text{quad}}(\lambda) = c_0 + c_1\lambda + c_2\lambda^2 \\
 \text{Exponential extrapolation :} & \quad \bar{p}^{\text{exp}}(\lambda) = c_0 + c_1e^{-c_2\lambda} \\
 \text{Richardson extrapolation :} & \quad \bar{p}^{\text{Rich}}(\lambda) = c_0 + c_1\lambda + \dots + c_n\lambda^n
 \end{aligned} \tag{18}$$

where  $c_0, c_1, \dots, c_n$  are the unknown coefficients. The linear, quadratic and Richardson extrapolations all belong to polynomial models. The difference lies in that the highest order of linear and quadratic extrapolations are fixed, while the highest order of the Richardson  $n$  is related to the number of elements in the estimated probabilities  $\hat{\mathbf{p}} = \{\hat{p}_0, \hat{p}_1, \dots, \hat{p}_n\}$ . For example, the Richardson extrapolation will degenerate into the linear one when  $n = 1$ , and will degenerate into the quadratic one when  $n = 2$ . The coefficients of these models are determined via the least squares fitting, i.e., finds optimal coefficients that minimize the sum of squared residuals  $\sum_{i=0}^n (\hat{p}_i - \bar{p}(\lambda = 1 + 2i))^2$ . Then the noiseless value can be predicted by  $\bar{p}(\lambda = 0)$ . Finally, the mitigated distance  $\bar{d}$  is obtained by

$$\bar{d} = 4Z(\bar{p}(\lambda = 0) - \frac{1}{2}) \tag{19}$$

The performance of these extrapolation models will be validated in Section 3.1. We would like to mention that ZNE can only handle the hardware noise associated with quantum gates. In fact, there exists another type of noise called shot noise, which arises from the statistical estimation of  $\hat{p}$  from the measurements [5]. A straightforward illustration of the shot noise is presented in Figure 3, where the blue intervals associated with the estimated  $\hat{p}$  are used to present the shot noise. The shot noise is influenced by the number of measurements  $n_s$ , where a larger value of  $n_s$  leads to lower shot noise, resulting in a higher accuracy of the estimated  $\hat{p}$ . The influence of  $n_s$  on error mitigation will be discussed later in Section 3.1. The flowchart of the distance calculation via error-mitigated quantum computing is detailed in Algorithm 1.

---

**Algorithm 1** distance calculation via error-mitigated quantum computing

---

**Require:** Vectors  $\mathbf{V}$ ,  $\mathbf{V}'$ ;  $Z = \|\mathbf{V}\|^2 + \|\mathbf{V}'\|^2$ ; Number of measurements  $n_s$ ;  
Maximum folding number  $n$

**Step 1: Noise-scaling**

**for**  $i = 0$  to  $n$  **do**

Fold each quantum gate of the swap test circuit  $i$  times

Save the noise scale factor  $\lambda = 1 + 2i$  to the set  $\boldsymbol{\lambda}$

**for**  $t = 1$  to  $n_s$  **do**

Encode  $|\phi\rangle$  and  $|\psi\rangle$  into the quantum computer via qRAM

Run the circuit and measure the first qubit

**end for**

Set  $n_0$  as the number of 0s in the measurement results

Estimate the probability  $\hat{p} = n_0/n_s$  and save it to the set  $\hat{\boldsymbol{p}}$

**end for**

**Step 2: Extrapolation**

Choose an extrapolation model  $\bar{p}(\lambda)$

Fit  $\bar{p}(\lambda)$  with  $\hat{\boldsymbol{p}}$  and  $\boldsymbol{\lambda}$

Extrapolate the noiseless value  $\bar{p}(\lambda = 0)$

Compute the mitigated distance  $\bar{d} = 4Z(\bar{p}(\lambda = 0) - \frac{1}{2})$

---

### 3 Validation

In this section, numerical tests are carried out to validate the proposed data-driven method with error-mitigated quantum computing (referred to as mitigated qDD). First, we will show the performance of different extrapolation models within ZNE in distance calculation. Then, a roof truss structure is used to validate the effectiveness of the mitigated qDD. Since the availability of real quantum computers is limited currently, the numerical tests in this paper are all carried out based on the quantum computer simulator Qpanda developed by Origin Quantum [38]. To simulate the hardware noise in quantum computer, each gate of the swap test circuit is associated with depolarizing noise shown in Eq. (11). For all the numerical examples in this paper, the noise parameter  $q$  is set as 0.05. In addition, we use the normal approximation to accelerate the statistical estimation of  $\hat{p}$  on the quantum computer simulator, as shown in Appendix A.

### 3.1 Validation of the error mitigation

In this section, we will evaluate the performance of the four extrapolation models from Eq. (18) in improving the accuracy of distance calculation. We first randomly sample 1000 vector pairs  $(\mathbf{V}_1, \mathbf{V}_2)$  in a 6-dimensional space, and their distances  $d = (\mathbf{V}_1 - \mathbf{V}_2)^2$  obey the uniform distribution. The linear, quadratic, exponential, and Richardson extrapolation models are used to predict noiseless probabilities and then calculate the mitigated distances. The maximum folding number  $n$  is set as 6, which means  $\lambda = \{1, 3, \dots, 13\}$  and  $\hat{\mathbf{p}} = \{\hat{p}_0, \hat{p}_1, \dots, \hat{p}_6\}$  are used to fit each extrapolation model  $\bar{p}(\lambda)$ . The number of measurements  $n_s$  is set as  $10^{12}$ .

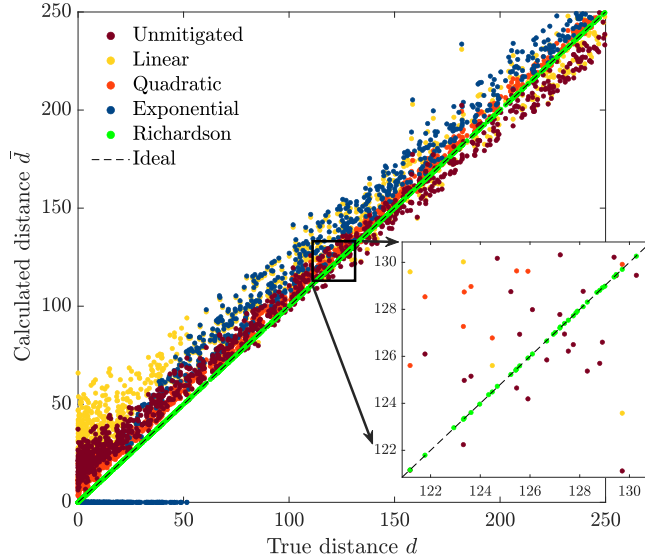


Figure 4: True distances versus calculated distances.

Figure 4 represents the true distances versus calculated distances from the 1000 vector pairs. As a reference, the dashed line marked with ‘Ideal’ is drawn followed by the relation  $\bar{d} = d$ , meaning points closer to the dashed line represent higher accuracy results. The distances calculated without error mitigation marked with ‘Unmitigated’ show significant discrepancies from the dashed line, indicating a notable error. Meanwhile, the accuracy of Richardson extrapolation outperforms the accuracy of the other three extrapolation models. To quantitatively analyze the performance of these extrapolation models, the relative errors  $|\bar{d} - d|/d$  of the calculated distances  $\bar{d}$  are presented in Figure 5. While the linear, quadratic, and exponential extrapolations contribute only a slight or no improvement in the accuracy of distance calculation, the Richardson extrapolation exhibits a notable enhancement in accuracy, i.e., nearly decreasing the error from  $10^{-1}$  to  $10^{-4}$ . In conclusion, the results show that error mitigation with ZNE can effectively reduce the noise in distance calculation.

We then investigate the effect of  $n_s$  on the distance calculation with error-mitigated quantum computing, where a larger value of  $n_s$  leads to lower shot noise of estimated  $\hat{\mathbf{p}}$ , as mentioned in Section 2.3. The root mean squared error (RMSE) of distance  $d_{\text{RMSE}} = \sqrt{\frac{\sum(\bar{d}-d)^2}{1000}}$  is used to reflect the average accuracy. Figure 6 presents the influence of  $n_s$  on the RMSE for the four

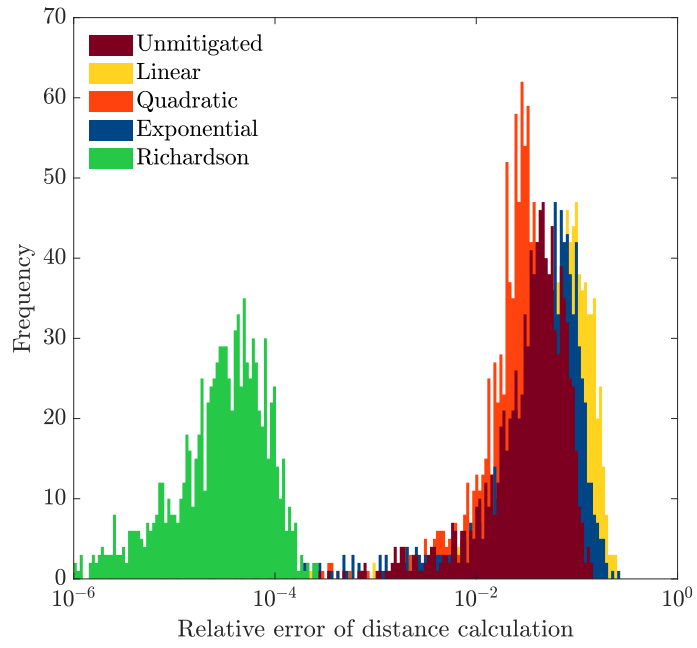


Figure 5: Frequency of the relative errors of distance calculations.

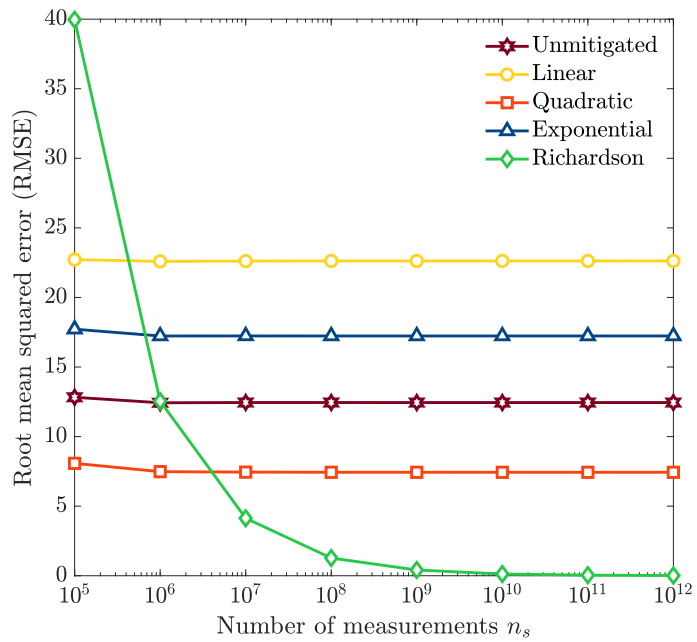


Figure 6: The number of measurements versus the root mean squared error (RMSE) of distance calculations.

extrapolation models. The accuracy of distance calculations improves with an increase in the value of  $n_s$  for all extrapolation models, though it is not obvious for the other three models except the Richardson. The reason is that the Richardson extrapolation has more unknown coefficients than the other three models. On one hand, it leads to a higher capacity to represent a complex relationship between  $\hat{p}$  and  $\lambda$ . On the other hand, it is more sensitive to the shot noise. Therefore, the Richardson extrapolation can accurately predict the noiseless  $\bar{p}(\lambda = 0)$  and the mitigated  $\bar{d}$  with a large  $n_s$ , and shows large errors in predicting the noiseless value with a small  $n_s$ . Furthermore, the influence of the maximum folding number  $n$  on the RMSE is investigated. As shown in Figure 7, the accuracy of the distance calculations with Richardson and exponential extrapolations reaches optimal at  $n = 6$ , whereas the one with linear and quadratic extrapolations decreases with increasing  $n$ . This implies that the performance of ZNE is sensitive to the maximum folding number  $n$ . We would like to mention that the optimal choice of  $n$  deserves future investigations [47].

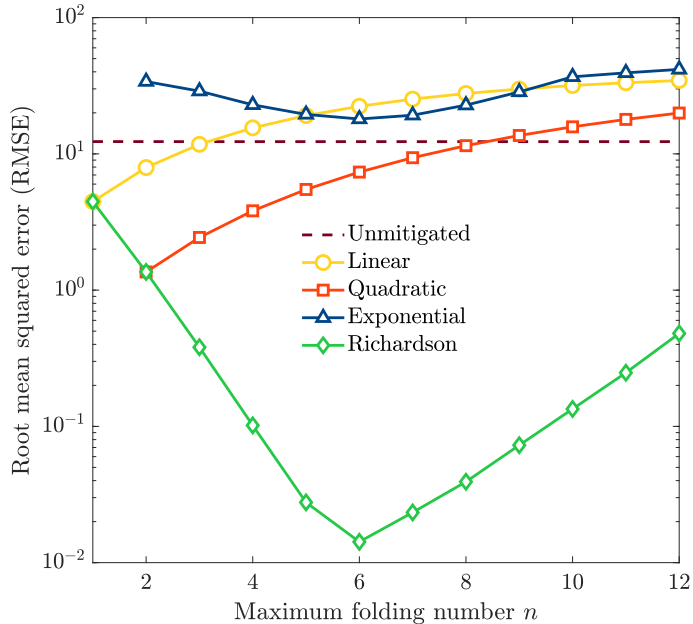


Figure 7: The maximum folding number  $n$  versus the root mean squared error (RMSE) of distance calculations.

In conclusion, the Richardson extrapolation with  $n_s \geq 10^7$  and the maximum folding number  $n = 6$  shows good performance in distance calculations based on noisy quantum computing. Therefore, the Richardson extrapolation is utilized for error mitigation in the subsequent numerical examples.

### 3.2 Roof truss

In this section, a roof truss with 11 bars and 7 nodes is considered to validate the performance of ZNE in data-driven simulation with noisy quantum computing. The configuration of the roof truss is shown in Figure 8. All the bars have the same cross-sectional area  $A = 100 \text{ mm}^2$ . The displacement of node 1 is fixed in the  $x$  and  $y$  directions, while the node 7 is fixed in the  $y$

direction. The nodes 2, 4 and 6 are under the loads  $P = 200$  N.

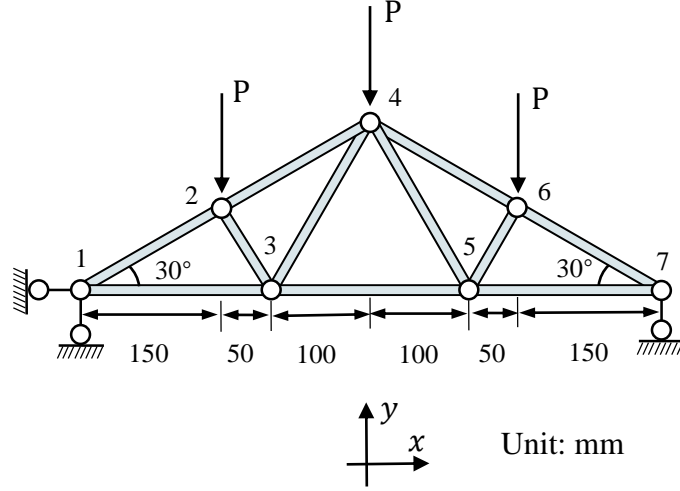


Figure 8: Sketch of the roof truss.

The material of the roof is assumed to satisfy a Ramberg-Osgood material model, and the material database is collected by uniformly sampling the stress data in the range  $\sigma \in [-6, 6]$  MPa and obtaining the corresponding strain data  $\epsilon$  via the following relation

$$\epsilon = \frac{\sigma}{E} + \alpha \frac{\sigma}{E} \left( \frac{|\sigma|}{\sigma_0} \right)^{\beta-1} \quad (20)$$

where  $E = 10000$  MPa refers to the Young's modulus,  $\alpha = 0.5$  the yield offset,  $\sigma_0 = 5$  MPa the yield stress and  $\beta = 3$  the hardening exponent. Furthermore, the  $k$ -d tree data structure is used to reduce the number of distance calculations in data-driven computing. The analytical solution is used as the reference result, and root-mean-square (RMS) error of stress  $\sigma_{\text{RMS}}$  is employed to evaluate the accuracy of solutions

$$\sigma_{\text{RMS}} = \sqrt{\frac{\sum_{e=1}^m w_e (\sigma_e - \sigma_e^{\text{ref}})^2}{\sum_{e=1}^m w_e (\sigma_e^{\text{ref}})^2}} \quad (21)$$

Firstly, the performance of the data-driven methods based on classical computing (classical DD), noisy quantum computing (unmitigated qDD), and error-mitigated quantum computing (mitigated qDD) are evaluated, where the material database with 161 data is used. Figure 9 presents the evolution of global distances  $\bar{\mathcal{F}} = \frac{1}{2} \sum_{e=1}^m w_e \bar{\mathcal{F}}_e(\bar{\mathbf{z}}_e, \bar{\mathbf{z}}_e^*)$  during the data-driven computing process, which is defined as the sum of the distances for all the integral points [6]. The mitigated qDD can accurately predict the stress of each bar ( $\sigma_{\text{RMS}} = 0.87\%$ ), whose precision compared to that of classical DD ( $\sigma_{\text{RMS}} = 0.92\%$ ). Although unmitigated qDD also has converged, the obtained result shows noticeable discrepancies in comparison to the reference solution ( $\sigma_{\text{RMS}} = 8.27\%$ ). This means ZNE can effectively improve the accuracy of quantum-

enhanced data-driven computing.

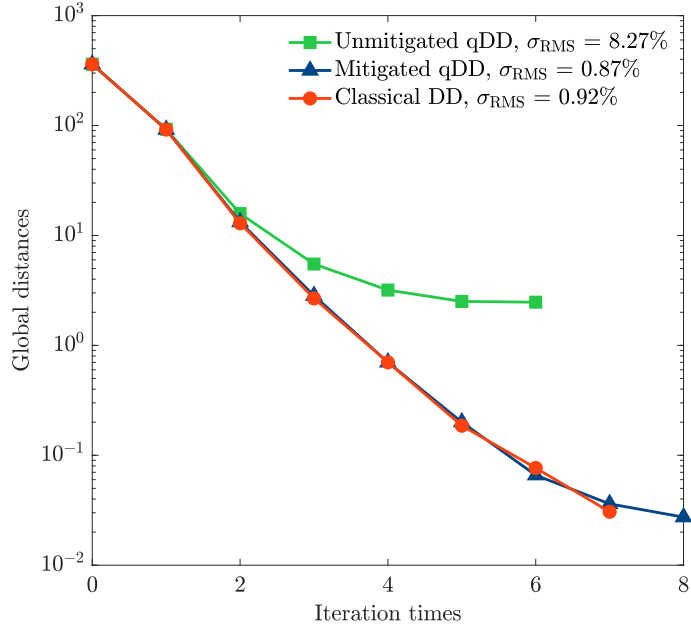


Figure 9: The global distances obtained by unmitigated qDD, mitigated qDD and classical DD.

Furthermore, the effectiveness of  $k$ -d tree data structure in accelerating data-driven computing is verified. Figure 10 shows the RMS error of stress and average number of distance calculations per nearest-neighbor search versus the number of data in the database. Compared to the full database without data structure, the  $k$ -d tree database can achieve the same level of accuracy while significantly reducing the number of distance calculations. We would like to emphasize that the results show a probability of combining a variety of efficient data structures [23, 36, 37, 48] with qDD, resulting in accelerations in both the number of data  $N$  and the dimension  $D$ .

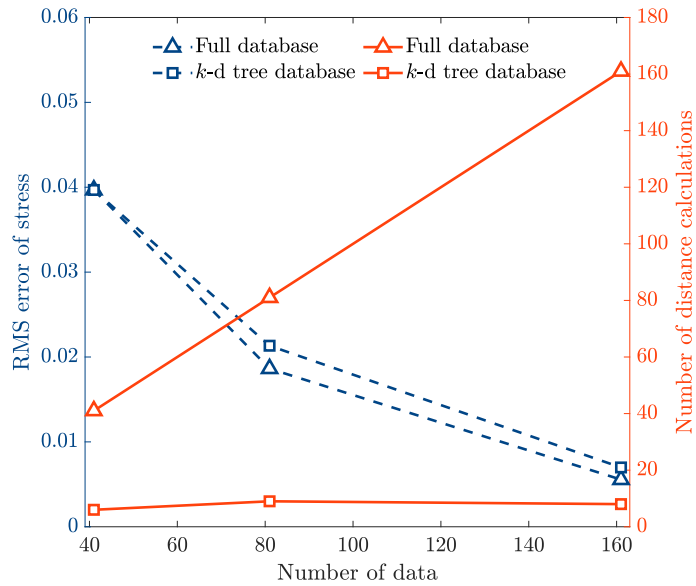


Figure 10: Performance of  $k$ -d tree database compared with the full database.

Finally, the influence of the number of measurements  $n_s$  on the mitigated qDD is investigated. As shown in Table 1, the value of  $n_s$  will affect the accuracy of mitigated qDD but has almost no effect on the unmitigated qDD. This can be explained by the relation between  $n_s$  and the accuracy of distance calculation (see Figure 6), where the mitigated distance with Richardson is sensitive to  $n_s$ , while the unmitigated distance is almost unaffected by  $n_s$ . Since the main idea of the data-driven computing is to find the material data  $\bar{\mathbf{z}}_e^*$  that closest to the admissible state  $\bar{\mathbf{z}}_e$ , the accuracy of the calculated distance between  $\bar{\mathbf{z}}_e^*$  and  $\bar{\mathbf{z}}_e$  will directly influence the nearest-neighbor search, thereby affecting the performance of data-driven computing.

In a word, the error mitigation with ZNE can improve the performance of quantum computing in data-driven simulation.

Table 1: Root-mean-square (RMS) error of stress versus the number of measurements  $n_s$  for the mitigated and unmitigated qDD. The classical DD is used as a reference.

Classical DD	0.92%		
	$n_s = 10^8$	$n_s = 10^{10}$	$n_s = 10^{12}$
Mitigated qDD	5.13%	1.93%	0.87%
UnMitigated qDD	8.24%	8.09%	8.27%

## 4 Application: composite L-shaped beam

In this section, the proposed method is applied in the data-driven multiscale simulation of a composite L-shaped beam. In data-driven multiscale simulation, the computations are conducted at microscopic and macroscopic scales separately [8]. The microscopic problem is solved offline to construct the material database  $\bar{\mathcal{D}}$ , where the stress-strain data is collected through computational homogenization on the representative volume element (RVE), as presented in Appendix C. The macroscopic problem is then solved online using data-driven computing, and the material behavior is directly provided by the material database. Compared to the traditional multiscale finite element method (FE<sup>2</sup>) [49], the data-driven multiscale simulation can significantly reduce the online computational cost while ensuring the accuracy [8]. Here, quantum computing is employed to improve the data-driven multiscale simulation at macroscopic scale, and the effect of hardware noise on quantum computing will be mitigated via ZNE.

The macroscopic configuration of the L-shaped beam is shown in Figure 11, as well as the RVE at the microscopic scale. The beam is subjected to a concentrated load  $F = 1000$  N/mm on the right edge and a fixed constraint on the upper edge. The microstructure of the beam consists of the inclusion and the matrix, both of which are assumed to satisfy the Ramberg-Osgood constitutive relation

$$E\boldsymbol{\epsilon} = (1 + \nu)\tilde{\boldsymbol{\sigma}} - (1 - 2\nu)p\mathbf{I} + \frac{3}{2}\alpha\left(\frac{\sigma_M}{\sigma_0}\right)^{\beta-1}\tilde{\boldsymbol{\sigma}} \quad (22)$$

where  $\nu$  represents the Poisson's ratio,  $\tilde{\boldsymbol{\sigma}} = \boldsymbol{\sigma} + p\mathbf{I}$  denote the stress deviator,  $p = -\frac{1}{3}\boldsymbol{\sigma} : \mathbf{I}$  is the



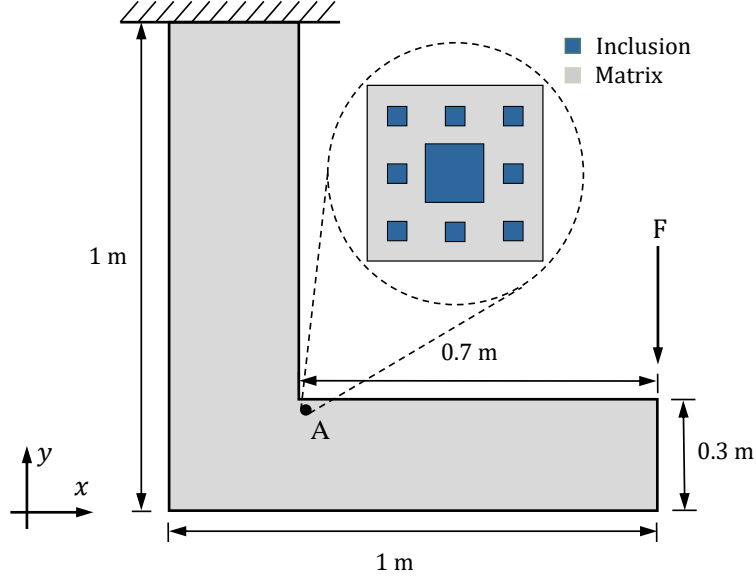


Figure 11: Sketch of the L-shaped beam.

equivalent hydrostatic stress,  $\sigma_M$  expresses the Mises equivalent stress. The material properties of the inclusion and the matrix are given in Table 2. To generate the material database, we uniformly sample the macroscopic strains in ranges  $\bar{\epsilon}_{xx} \in [-0.015, 0.030]$ ,  $\bar{\epsilon}_{yy} \in [-0.025, 0.040]$ , and  $\bar{\epsilon}_{xy} \in [-0.015, 0.010]$ . Then the macroscopic stresses are computed through computational homogenization on the RVE, resulting in  $100^3$  data.

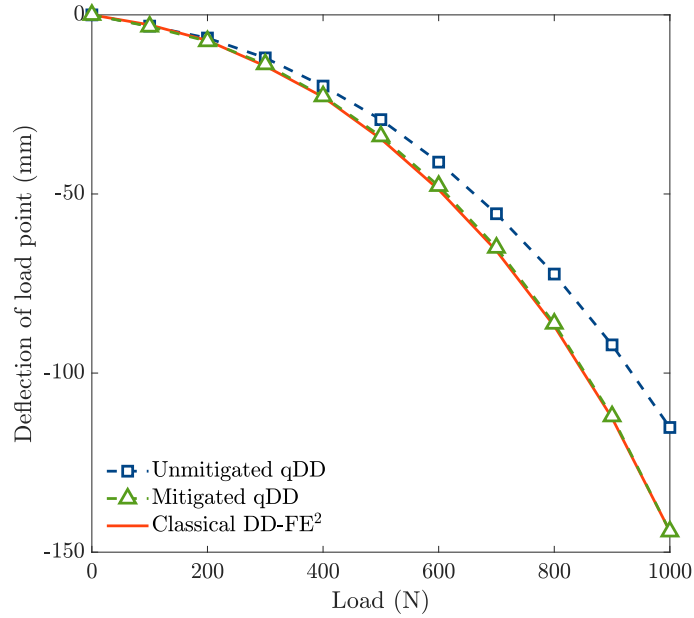


Figure 12: Deflection of the load point versus the external load.

For the computation at the macroscopic scale, the mitigated qDD and unmitigated qDD are applied. As a reference, the data-driven FE<sup>2</sup> method with the classical computer (referred to as classical DD-FE<sup>2</sup>) is used to solve the same problem. Figure 12 shows the load-deflection curve of the load point. The mitigated qDD can accurately predict the deflection of the load point

Table 2: Material parameters of the inclusion and the matrix.

	$E$ (MPa)	$\sigma_0$ (MPa)	$\nu$	$\alpha$	$\beta$
Inclusion	$10^5$	100	0.3	0.5	3
Matrix	$10^4$	10	0.3	0.5	3

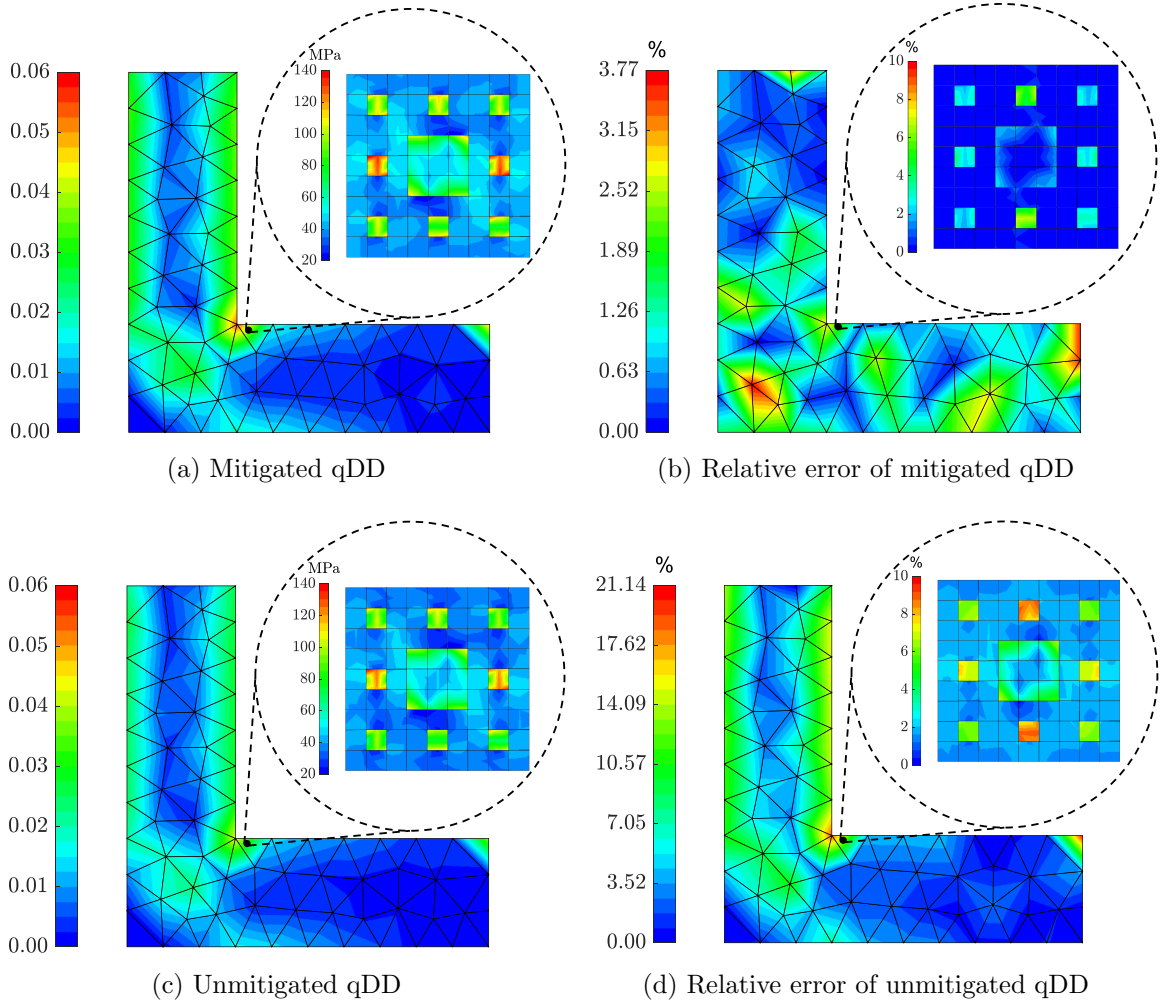


Figure 13: Strain fields  $\sqrt{3J_2}$  and the corresponding relative errors for the L-shaped beam, as well as the von Mises stress fields and the corresponding relative errors for the RVE at the integration point. The solutions of classical DD-FE<sup>2</sup> are used as a reference.

under various loads, while unmitigated qDD exhibits around 20% relative errors. Figure 13 shows the strain fields  $\sqrt{3J_2}$  and the corresponding relative errors at the macroscopic scale under the load  $F = 1000\text{N/mm}$ , as well as the von Mises stress fields and the corresponding relative errors at the microscopic scale. Compared to the unmitigated qDD, the relative error of the stress field at the microscopic scale is notably reduced, and the maximum relative error at the macroscopic scale is reduced from 21.14% to 3.77%. In a word, the mitigated qDD exhibits higher accuracy compared to unmitigated qDD at both microscopic and macroscopic scales. This validates the effectiveness of the error-mitigated quantum computing in data-driven simulation, even for composite materials and structures.

## 5 Conclusion

In realizing practical applications of quantum computing in data-driven computational mechanics, hardware noise is an unavoidable problem for NISQ quantum computers. We use zero-noise extrapolation (ZNE) to deal with this issue, which helps increase the accuracy of distance calculations and makes quantum computing perform better in data-driven computing. We also combine the quantum algorithm with the  $k$ -d tree data structure, making the distance calculations even more efficient. Numerical examples confirm the effectiveness of ZNE in reducing the distance calculation error, and validation on a roof structure demonstrates improved accuracy in data-driven computing. The application to a composite L-shaped beam highlights the role of ZNE in enhancing the overall accuracy of quantum computing for data-driven multiscale simulation.

We have identified several areas that need more research. One challenge is the current limit on the circuit depth of real quantum computers. Even though the swap test uses just three gates, making it run on a real device means breaking these gates down into simpler ones, such as single-qubit U gates and two-qubit CNOT gates [50]. This adds to the circuit depth, indicating that error mitigation experiments for distance calculation on real quantum computers call for more advanced hardware devices. Also, we might have to think about using a more complex noise model like the sparse Pauli-Lindblad noise model. This would mean exploring new extrapolation methods [33,51], or even different error mitigation techniques like probabilistic error cancellation (PEC) [30]. Lastly, another challenge is the task of encoding classical data into quantum computers [52,53], which requires additional evaluation of associated potential errors, as pointed out in [54]. Addressing these issues will enhance the capability of quantum computing and open an avenue for its practical application in data-driven computational mechanics.

## Acknowledgements

This work has been supported by the National Natural Science Foundation of China (Grant No. 11920101002), the National Key R&D Program of China (Grant No. 2022YFE0113100) and the National Natural Science Foundation of China (Grant Nos. 12172262 and 12202322).

## Appendix A Normal approximation

To estimate the probability  $\hat{p} = n_0/n_s$ , we need to run the quantum circuit  $n_s$  times, and then get the number of  $|0\rangle$  in the measurement results  $n_0$ . This process is time-consuming when numerically conducted on a quantum computer simulator. Since one measurement related to state  $|0\rangle$  with probability  $p$  and state  $|1\rangle$  with probability  $1 - p$ ,  $n_0$  follows a binomial distribution  $n_0 \sim B(n_s, p)$ . According to the central limit theorem, the distribution of  $n_0$  becomes approximately normal with  $n_0 \sim N(n_s p, n_s p(1 - p))$  if both  $n_s p$  and  $n_s(1 - p)$  are larger than 5. Hence, when the estimation of  $p$  is performed through a quantum computer simulator, it can be achieved by generating a random variable that obeys the corresponding normal distribution, which reduces the computational complexity of estimating  $p$  from  $O(n_s)$  to  $O(1)$ .

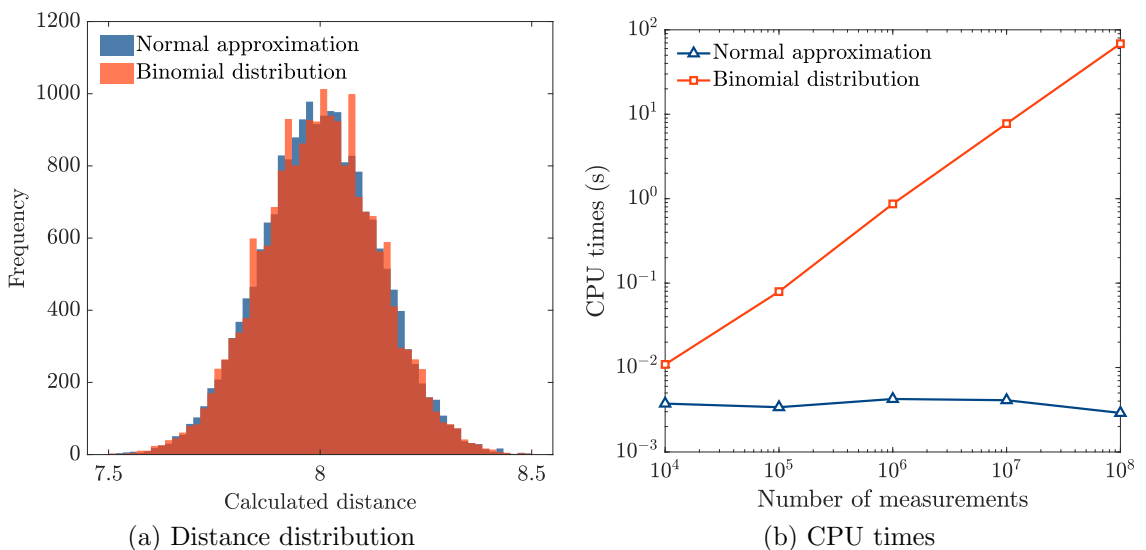


Figure 14: Performance of the normal approximation in comparison to the binomial distribution.

Two numerical tests are conducted to verify the effectiveness and efficiency of the estimation method with normal approximation. Firstly, the distances between vectors  $(0, 2)$  and  $(2, 0)$  are calculated based on normal approximation and binomial distribution, where the number of measurements is set as  $n_s = 10^5$  and 20000 samples of distances are included. As shown in Figure 14 (a), the distance distribution obtained by normal approximation is similar to the one obtained by the binomial distribution. This means the estimation method with normal approximation retains the same statistical characteristics as the one with binomial distribution. Then, the computational times of both the two estimation methods versus the number of measurements  $n_s$  are tested. As shown in Figure 14 (b), the required computational time for normal approximation is independent of  $n_s$ , which shows its significant efficiency advantage.

## Appendix B $k$ -d tree data structure

The  $k$ -d tree data structure accelerates the nearest-neighbor search by reducing the number of queries. In this section, we provide a brief overview of the  $k$ -d tree data structure. For a more

comprehensive understanding, interested readers can refer to [35, 37, 39] for in-depth details.

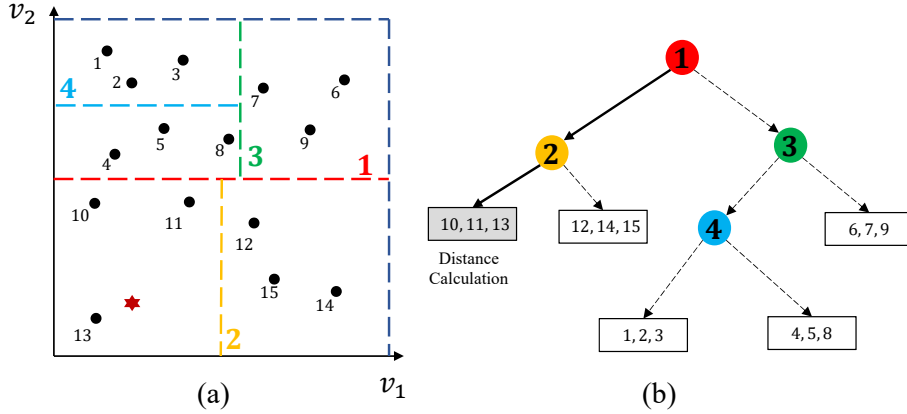


Figure 15: Diagrams of a two-dimensional  $k$ -d tree data structure. (a) Space partitioning. (b) Corresponding binary tree.

The idea behind constructing a  $k$ -d tree data structure is to partition the space using axis-aligned planes. In Figure 15 (a), we provide an example of space partitioning for 15 data points in two dimensions. The first plane, indicated by the red dashed line labeled as ‘1’, splits the data into two subsets. This initial split serves as the root node of the data structure shown in (b). The value of  $v_2$  for this line is determined by calculating the median of the  $v_2$  values of all the data points. Subsequently, the resulting two subsets are further split using lines ‘2’ and ‘3’ in a similar way. The  $v_1$  values for these lines are determined by calculating the median of the  $v_1$  values within their respective subsets, resulting in two leaf nodes. This recursive splitting process continues until the number of data points in a subset falls below a specified threshold, which is set to 3 in this example. It is important to note that the construction of the tree structure is performed offline, thereby not adding to the computational cost during online operations.

To locate the nearest neighbor of a query data point, the search begins from the root node and proceeds down to the leaf nodes. An example query is also illustrated in Figure 15 (a) and (b), with the query data point denoted by the red hexagon in (a). The query route shown in (b) initiates at the root node ‘1’ and then progresses to the leaf node ‘2’. Finally, distance calculations are executed between the query data point and the data points marked as ‘10’, ‘11’, and ‘13’, resulting in the final nearest neighbor. In this work, the quantum algorithm performs distance calculations with error mitigation.

## Appendix C Microscopic problem

In the computational framework of data-driven multiscale simulation, the aim of the microscopic problem is to construct the material database denoted by  $\bar{\mathcal{D}}$  via homogenization computing on the RVE of the composite [8, 10]. The microscopic Cauchy stress  $\sigma$  and its conjugate

strain  $\epsilon$  are adopted, and the microscopic homogenization problem is formulated by:

$$\int_{\omega} \boldsymbol{\sigma} : \delta \epsilon d\omega = 0 \quad (23a)$$

$$d\boldsymbol{\sigma} = \mathbb{C}_t^{(r)} : d\epsilon \quad (23b)$$

$$\mathbf{u}^+ - \mathbf{u}^- = \bar{\boldsymbol{\epsilon}} \cdot (\mathbf{X}^+ - \mathbf{X}^-) \quad (23c)$$

$$\bar{\boldsymbol{\sigma}} = \frac{1}{|\omega|} \int_{\omega} \boldsymbol{\sigma} d\omega \quad (23d)$$

where  $\omega$  is the domain of the RVE,  $\mathbb{C}_t^{(r)}$  is the constitutive tensor of each material phase  $r$ . Eq. (23c) is the periodic boundary condition (PBC), which loads the macroscopic strain  $\bar{\boldsymbol{\epsilon}}$  to the boundary of RVE. The displacement is denoted by  $\mathbf{u}$ , the superscripts ‘+’ and ‘-’ specify two opposite surfaces of the RVE, and  $\mathbf{X}$  is the coordinate of the material point. Once  $\bar{\boldsymbol{\epsilon}}$  is given, Eqs. (23a) to (23c) can be solved using the Newton-Raphson method to get the deformed RVE. In post-processing, Eq. (23d) is used to compute the macroscopic Cauchy stress  $\bar{\boldsymbol{\sigma}}$ . In this manner, homogenized stress-strain data  $(\bar{\boldsymbol{\epsilon}}, \bar{\boldsymbol{\sigma}})$  can be generated and stored in the database  $\bar{\mathcal{D}}$ .

## References

- [1] A. Montanaro, S. Pallister, Quantum algorithms and the finite element method, *Physical Review A* 93 (3) (2016) 032324.
- [2] O. M. Raisuddin, S. De, FEqa: Finite element computations on quantum annealers, *Computer Methods in Applied Mechanics and Engineering* 395 (2022) 115014.
- [3] Z. Meng, Y. Yang, Quantum computing of fluid dynamics using the hydrodynamic Schrödinger equation, *Physical Review Research* 5 (3).
- [4] B. Liu, M. Ortiz, F. Cirak, Towards quantum computational mechanics, arXiv preprint arXiv:2312.03791.
- [5] Y. Xu, J. Yang, Z. Kuang, Q. Huang, W. Huang, H. Hu, Quantum computing enhanced distance-minimizing data-driven computational mechanics, *Computer Methods in Applied Mechanics and Engineering* 419 (2024) 116675.
- [6] T. Kirchdoerfer, M. Ortiz, Data-driven computational mechanics, *Computer Methods in Applied Mechanics and Engineering* 304 (2016) 81–101.
- [7] K. Karapiperis, L. Stainier, M. Ortiz, J. Andrade, Data-driven multiscale modeling in mechanics, *Journal of the Mechanics and Physics of Solids* 147 (2021) 104239.
- [8] R. Xu, J. Yang, W. Yan, Q. Huang, H. Hu, Data-driven multiscale finite element method: From concurrence to separation, *Computer Methods in Applied Mechanics and Engineering* 363 (2020) 112893.

- [9] J. Yang, R. Xu, H. Hu, Q. Huang, W. Huang, Structural-Genome-Driven computing for composite structures, *Composite Structures* 215 (2019) 446–453.
- [10] Y. Xu, J. Yang, X. Bai, Q. Huang, N. Damil, H. Hu, Material database construction for data-driven computing via a continuous path-following method, *Composite Structures* (2023) 117187.
- [11] W. Huang, R. Xu, J. Yang, Q. Huang, H. Hu, Data-driven multiscale simulation of FRP based on material twins, *Composite Structures* 256 (2021) 113013.
- [12] W. Yan, W. Huang, Q. Huang, J. Yang, G. Giunta, S. Belouettar, H. Hu, Data-driven multiscale method for composite plates, *Computational Mechanics* 70 (5) (2022) 1025–1040.
- [13] T. Kirchdoerfer, M. Ortiz, Data-driven computing in dynamics, *International Journal for Numerical Methods in Engineering* 113 (11) (2018) 1697–1710.
- [14] X. Bai, J. Yang, W. Yan, Q. Huang, S. Belouettar, H. Hu, A data-driven approach for instability analysis of thin composite structures, *Computers & Structures* 273 (2022) 106898.
- [15] Z. Kuang, X. Bai, Q. Huang, J. Yang, W. Huang, S. Belouettar, H. Hu, Data-driven computational framework for snap-through problems, *International Journal of Solids and Structures* 269 (2023) 112226.
- [16] P. Carrara, L. De Lorenzis, L. Stainier, M. Ortiz, Data-driven fracture mechanics, *Computer Methods in Applied Mechanics and Engineering* 372 (2020) 113390.
- [17] P. Carrara, M. Ortiz, L. De Lorenzis, Data-driven rate-dependent fracture mechanics, *Journal of the Mechanics and Physics of Solids* 155 (2021) 104559.
- [18] H. Dal, F. A. Denli, A. K. Acan, M. Kaliske, Data-driven hyperelasticity, Part I: A canonical isotropic formulation for rubberlike materials, *Journal of the Mechanics and Physics of Solids* 179 (2023) 105381.
- [19] O. Z. Tikenogulları, A. K. Acan, E. Kuhl, H. Dal, Data-driven hyperelasticity, Part II: A canonical framework for anisotropic soft biological tissues, *Journal of the Mechanics and Physics of Solids* 181 (2023) 105453.
- [20] J. Yang, W. Huang, Q. Huang, H. Hu, An investigation on the coupling of data-driven computing and model-driven computing, *Computer Methods in Applied Mechanics and Engineering* 393 (2022) 114798.
- [21] J. Yang, P. Li, Y. Zhang, Y. Hui, L. Xu, N. Damil, H. Hu, Unified functional based data-model-coupling computing for composite materials and structures, *Composite Structures* 312 (2023) 116840.
- [22] S. Wattel, J.-F. Molinari, M. Ortiz, J. Garcia-Suarez, Mesh d-refinement: A data-based computational framework to account for complex material response, *Mechanics of Materials* 180 (2023) 104630.

- [23] R. Eggersmann, L. Stainier, M. Ortiz, S. Reese, Efficient data structures for model-free data-driven computational mechanics, *Computer Methods in Applied Mechanics and Engineering* 382 (2021) 113855.
- [24] P. W. Shor, Fault-tolerant quantum computation, in: *Proceedings of 37th conference on foundations of computer science*, IEEE, 1996, pp. 56–65.
- [25] M. A. Nielsen, I. L. Chuang, *Quantum Computation and Quantum Information*, 10th Edition, Cambridge University Press, USA, 2011.
- [26] National Academies of Sciences, Engineering, and Medicine, *Quantum computing: progress and prospects*, National Academies Press, 2018.
- [27] D. A. Lidar, T. A. Brun, *Quantum error correction*, Cambridge University Press, 2013.
- [28] J. Preskill, Quantum computing in the NISQ era and beyond, *Quantum* 2 (2018) 79.
- [29] S. Endo, S. C. Benjamin, Y. Li, Practical quantum error mitigation for near-future applications, *Physical Review X* 8 (3) (2018) 031027.
- [30] K. Temme, S. Bravyi, J. M. Gambetta, Error mitigation for short-depth quantum circuits, *Physical Review Letters* 119 (18) (2017) 180509.
- [31] Y. Li, S. C. Benjamin, Efficient variational quantum simulator incorporating active error minimization, *Physical Review X* 7 (2) (2017) 021050.
- [32] A. Kandala, K. Temme, A. D. Córcoles, A. Mezzacapo, J. M. Chow, J. M. Gambetta, Error mitigation extends the computational reach of a noisy quantum processor, *Nature* 567 (7749) (2019) 491–495.
- [33] Y. Kim, A. Eddins, S. Anand, K. X. Wei, E. Van Den Berg, S. Rosenblatt, H. Nayfeh, Y. Wu, M. Zaletel, K. Temme, et al., Evidence for the utility of quantum computing before fault tolerance, *Nature* 618 (7965) (2023) 500–505.
- [34] D. Castelvechi, IBM quantum computer passes calculation milestone, *Nature* 618 (7966) (2023) 656–657.
- [35] J. H. Friedman, J. L. Bentley, R. A. Finkel, An algorithm for finding best matches in logarithmic expected time, *ACM Transactions on Mathematical Software (TOMS)* 3 (3) (1977) 209–226.
- [36] J. Yang, X. Bai, W. Yan, W. Huang, Q. Huang, Q. Shao, H. Hu, An efficient hierarchical data searching scheme for data-driven computational mechanics, *Chinese Journal of Solid Mechanics* 42 (3) (2021) 241–248.
- [37] B. Bahmani, W. Sun, A kd-tree-accelerated hybrid data-driven/model-based approach for poroelasticity problems with multi-fidelity multi-physics data, *Computer Methods in Applied Mechanics and Engineering* 382 (2021) 113868.



- [38] M. Dou, T. Zou, Y. Fang, J. Wang, D. Zhao, L. Yu, B. Chen, W. Guo, Y. Li, Z. Chen, et al., Qpanda: high-performance quantum computing framework for multiple application scenarios, arXiv preprint arXiv:2212.14201.
- [39] T. F. Korzeniewski, K. Weinberg, A multi-level method for data-driven finite element computations, *Computer Methods in Applied Mechanics and Engineering* 379 (2021) 113740.
- [40] V. Giovannetti, S. Lloyd, L. Maccone, Quantum random access memory, *Physical Review Letters* 100 (16) (2008) 160501.
- [41] V. Giovannetti, S. Lloyd, L. Maccone, Architectures for a quantum random access memory, *Physical Review A* 78 (5) (2008) 052310.
- [42] H. Buhrman, R. Cleve, J. Watrous, R. De Wolf, Quantum fingerprinting, *Physical Review Letters* 87 (16) (2001) 167902.
- [43] T. Giurgica-Tiron, Y. Hindy, R. LaRose, A. Mari, W. J. Zeng, Digital zero noise extrapolation for quantum error mitigation, in: *2020 IEEE International Conference on Quantum Computing and Engineering (QCE)*, IEEE, 2020, pp. 306–316.
- [44] C. King, The capacity of the quantum depolarizing channel, *IEEE Transactions on Information Theory* 49 (1) (2003) 221–229.
- [45] J. Vovrosh, K. E. Khosla, S. Greenaway, C. Self, M. S. Kim, J. Knolle, Simple mitigation of global depolarizing errors in quantum simulations, *Physical Review E* 104 (3) (2021) 035309.
- [46] V. R. Pascuzzi, A. He, C. W. Bauer, W. A. De Jong, B. Nachman, Computationally efficient zero-noise extrapolation for quantum-gate-error mitigation, *Physical Review A* 105 (4) (2022) 042406.
- [47] M. Krebsbach, B. Trauzettel, A. Calzona, Optimization of Richardson extrapolation for quantum error mitigation, *Physical Review A* 106 (6) (2022) 062436.
- [48] Z. Kuang, W. Yan, K. Yu, R. Xu, L. Li, Q. Huang, J. Yang, G. Giunta, S. Belouettar, Data-driven computing for nonlinear problems of composite structures based on sub-domain search technique, *Computers & Structures* 279 (2023) 106982.
- [49] F. Feyel, J.-L. Chaboche, FE<sup>2</sup> multiscale approach for modelling the elastoviscoplastic behaviour of long fibre SiC/Ti composite materials, *Computer methods in applied mechanics and engineering* 183 (3-4) (2000) 309–330.
- [50] L. Burgholzer, R. Raymond, R. Wille, Verifying results of the IBM Qiskit quantum circuit compilation flow, in: *2020 IEEE International Conference on Quantum Computing and Engineering (QCE)*, IEEE, 2020, pp. 356–365.
- [51] E. Van Den Berg, Z. K. Mineev, A. Kandala, K. Temme, Probabilistic error cancellation with sparse pauli–lindblad models on noisy quantum processors, *Nature Physics* (2023) 1–6.

- [52] S. Aaronson, Read the fine print, *Nature Physics* 11 (4) (2015) 291–293.
- [53] J. Biamonte, P. Wittek, N. Pancotti, P. Rebentrost, N. Wiebe, S. Lloyd, Quantum machine learning, *Nature* 549 (7671) (2017) 195–202.
- [54] R. LaRose, B. Coyle, Robust data encodings for quantum classifiers, *Physical Review A* 102 (3) (2020) 032420.